Solid Freeform Fabrication 2023: Proceedings of the 34th Annual International Solid Freeform Fabrication Symposium – An Additive Manufacturing Conference
Reviewed Paper

Spreading and Packing of Alumina Powder Using a Displacement-controlled Roller in SLFS

Kaya J. Bayazitoglu, Matthew Cassoli, Joseph J. Beaman, Desiderio Kovar

Center for Additive Manufacturing and Design Innovation and Department of Mechanical Engineering

University of Texas at Austin

Austin, TX, 78712

Abstract

Selective laser flash sintering (SLFS) is a powder bed fusion process that enables direct additive manufacturing of ceramics. Similar to other powder bed fusion processes, the density of the ceramic powder bed impacts attainable density of the final part. Experiments were conducted using a spray-dried alumina powder that was spread and then packed using a displacement-limited roller. The spreadability of the powder was visually assessed. The microstructure of the resulting compacted powder was compared to a traditional method of pressing ceramic powder into a pellet using a die and hydraulic press. Packed regions were sintered to final density and compared in a scanning electron microscope to samples hydraulically pressed at known pressure to evaluate the efficacy of a roller-based packing process.

Introduction

A number of existing indirect additive manufacturing (AM) methods for producing ceramics utilize packed powder beds including selective laser sintering (Sing, et al. 2017) and binder-jetting (Du, et al. 2020). Recently selective laser flash sintering (SLFS) has been proposed as a method for performing direct ceramic AM, either without a binder or with minimal binder. (Hagen, Kovar and Beaman, Effects of Electric Field on Selective Laser Sintering of Yttria-Stabilized Zirconia Ceramic Powder 2018) (Hagen, Beaman and Kovar, Selective laser flash sintering of 8-YSZ 2020) The lack of significant amounts of binder is significant because binder must be removed before the part can be sintered to full density and this pyrolysis step can be extremely slow for large bulk part shapes. A commonality between both SLFS and existing indirect AM methods is the density of the powder bed affects the subsequent sintering of the powder; the highest final densities are achieved when the powder bed has a high density. (Bruch 1962)

Budding and Vaneker studied the importance of powder bed density in ceramic AM, including three methods of spreading powder to induce the most compaction, (blade, and two direction of roller rotation) (Budding and Vaneker 2013). In this study a counter rotating roller was found to be most effective in compacting powder in powder bed. Past reviews of literature have also shown support for the counter rotating roller strategy (Du, et al. 2020).

Other studies showed that compacting ceramic powder beds could improve AM, but focused on spreadability of powder, in addition to bed density. (Li, Pei and Ma 2021) For example, Li et al. studied the formation of defects on the top of the powder bed after compaction with a roller over the course of many successive layers, as would be required for an AM process. They also used a spray-dried ceramic to enhance flowability of the powder. It was found that some levels of compaction caused very few defects to the top powder bed surface, while others caused surface waviness that got worse after a few layers before tapering. This study shows that compaction can influence the resulting surface quality of the green part and justifies that further studies are required to understand this phenomenon and how it affects the final density of parts.

In the present work, we study the viability of collapsing spray-dried ceramic powder with a simple roller and comparing achievable sintered density from a compressed powder bed. A simple roller device was fabricated to spread and compress a single layer of powder. The device was designed to manually compress powder using a displacement-controlled roller that could be implemented in any powder bed process. The sintered density of a part produced using this roller is compared to parts produced using a traditional uniaxial die pressing operation.

Materials and Methods

Feedstock

The powder used for sintering and compaction was a spray-dried alumina, (APA-RTP SB, Sasol North America, Tucson AZ) with a granule size of 55 μm and a bulk density of 1.15 g/cm^3. The powder had a mean primary particle size of 0.4 μm and an inorganic composition of 99.94% MgO-doped alumina. A small amount (3 wt%) of an acrylic is used to bind the primary particles into granules. Sasol recommends pressing the powder at 100 MPa (15,000 psi) to fully collapse the spray-dried granules, filling the inter-granule gaps, and resulting in a green density of 2.32 g/cm^3. This enables a final fired density of 3.95 g/cm^3.

Spray-dried alumina was selected because the large size and spherical shape of the spray-dried granules allows the powder to flow well and spread evenly without agglomeration that is endemic to sub-micron-scale powders. The low binder content allows for facile pyrolysis without bloating or cracking. Preliminary experiments revealed that the spray-dried alumina did not tend to stick to the steel roller, whereas experiments with various non-spray-dried ceramic powders showed a tendency to stick to the roller during the compaction step. For comparison, disk-shaped pellets were also produced via uniaxial die compaction at various pressures.

Die Compaction

A cylindrical die with a diameter of 25.4 mm (1 in) and two punches were used to uniaxial press the powders to produce control samples. Stearic acid was dissolved in acetone and the solution was then coated on the inside of a die and punches using a swab. The acetone was allowed to evaporate, leaving a thin layer of stearic acid that acted as a lubricant between the powder and the die. Individual powder samples with a mass of 4 g were uniaxially compacted in the die using a hydraulic press at 83 MPa (12,000 psi), 41 MPa (6,000 psi), 21 MPa (3,000 psi), and 10 MPa (1,500 psi). The green compacts were manually removed from the die after pressing.

Roller Experimental Apparatus

A rendering of the experimental apparatus is shown in Figure 1. A three-part setup was fabricated consisting of: a steel two inch diameter roller, an aluminum baseplate, and a flat, alumina bed plate. The aluminum roller had grooves machined in it to create the center section where the powder is placed and compressed. The ungrooved surfaces of the roller were turned so that each of these surfaces had the same diameter. The base plate had walls machined in it to align with the roller's grooves and guide the roller down its length. The outer faces of the base plate were machined so their thicknesses were the same. The ceramic plate was slip cast, dried and then fully sintered before surface grinding it to fit in the middle portion of the base plate. This removable plate allowed for easier inspection of compressed ceramic powder. Steel shims that were 0.102 mm (0.004 in) thick were stacked on the sides of the base plate which the roller sat on to limit the thickness of the rolled compact. The height of the roller above the bed plate was varied by changing the number of shims.

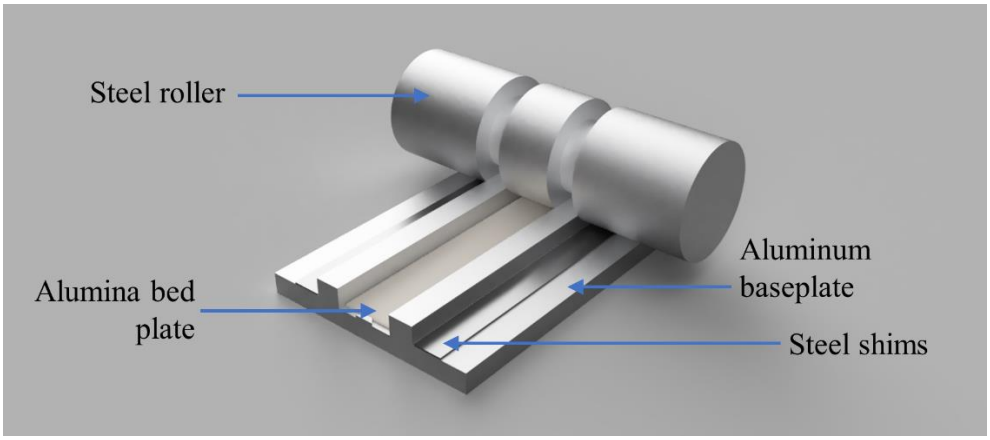

Figure 1: Experimental apparatus

Spreading Process

To spread powder, the distance between the powder and the ceramic plate was first set by adding or subtracting shims on the side of the base plate. Then, an amount of powder that was greater than required was placed in front of the roller such that excess powder would be pushed off the plate after the roller's full spreading movement. As has been performed in previous studies, the roller counter-rotated while spreading the powder. The leading edge of the roller moved in the same direction as the overall roller movement and upwards (Moghdasi, et al. 2021).

Compaction Process

After spreading, the powder was compacted to a specified level, shown in Table 1. A pre-determined number of shims were removed from the setup, reducing the distance between the roller and the ceramic plate, then the roller was manually pressed down while it was rolled across the powder bed. For this compression step, the roller co-rotated with its movement. The shims limited the maximum compaction that could be achieved by the roller. However, since the roll force was applied manually, the actual compaction was limited by the force that could be applied

by the operator. There was no additional instrumentation to measure the force applied by the operator.

Visual Inspection

After the compaction step, the roller and resulting powder bed were inspected for powder stuck on the roller, flatness, waviness, and any other features that might impact the ability to repeatably spread powder for hundreds of layers, as would be required for a powder bed AM process.

Pyrolysis and Sintering

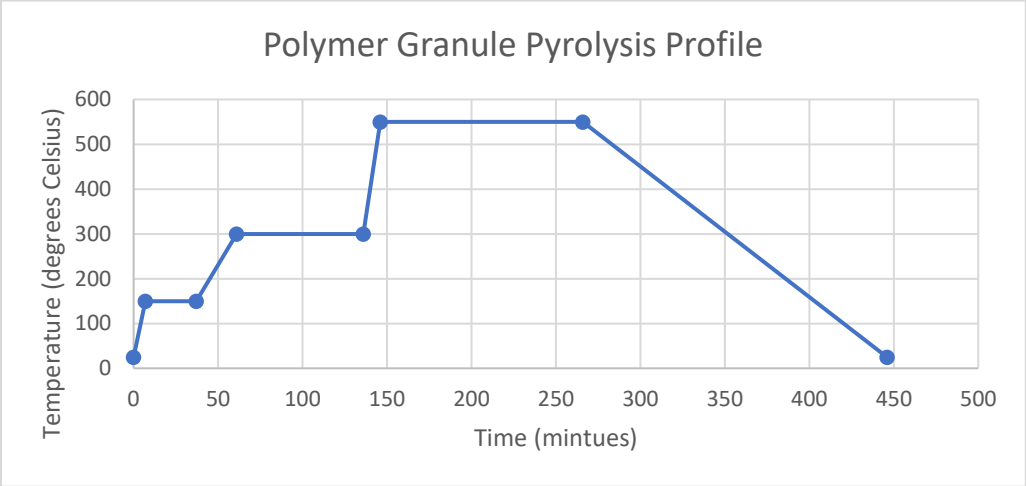

Figure 2: Pyrolysis profile for spray-dried powder

Compacted powder to be sintered was first transferred to a furnace for polymer pyrolysis according to the thermal profile shown in Figure 2. After polymer burnout, the alumina was conventionally sintered at 1510˚C. The furnace ramped to the dwell temperature at 5˚C/ minute and was held at the dwell temperature of 1510˚C for two hours. Both pyrolysis and sintering were performed in air.

Compaction Experiments

By supporting the roller using 5 shims, the powder was spread 0.508 mm (0.020”) above the surface of the ceramic plate using a counter-rotating motion of the roller. For each trial, shims were removed according to lower the roller. A co-rotating motion of the roller was used to pack the powder layer. The resulting powder bed was then visually inspected, and an attempt was made to collect a packed portion of the bed for sintering. For distances of 0.203 mm (0.008”) and 0.102 mm (0.004”), the experiment was displacement-controlled, as the shims constrained the roller above the ceramic plate. In the last two trials (3 and 4), shims were removed so that the roller was no longer constrained above the ceramic plate by the shims. Thus, the position of the roller was determined the amount of pressure that could be manually applied and the powder bed’s resistance.

Table 1: Rolling Trials

Trial #	Spread Height	Pack Height	Pack Distance
1	0.508 mm (0.020”)	0.203 mm (0.008”)	0.305 mm (0.012”)
2	0.508 mm	0.102 mm (0.004”)	0.406 mm (0.016”)
3	0.508 mm	0.000 mm (0.000”)	0.508 mm (0.020”)
4	0.508 mm	-0.102 mm (-.004”)	-0.102 mm (-0.024”)

SEM Characterization

Coupons taken from the powder bed from trial 4 of the powder bed compaction roller study, and from the compact from the die-pressed sampled were pyrolyzed and sintered as described above. Sintered alumina pieces were fractured and mounted in an SEM equipped with a tungsten-filament thermionic emitter. The resulting images were used to assess porosity and the level of collapse of the spray-dried granules.

Results and Discussion

Coupons were not collected from trials 1 and 2 because the green compacted powder were not strong enough to remain intact after minimal compaction. While some coupons were able to be retrieved from trial 3, these were extremely fragile and could not be analyzed further. Several coupons were retrieved from trial 4, some of which proceeded through pyrolysis, sintering, and SEM characterization.

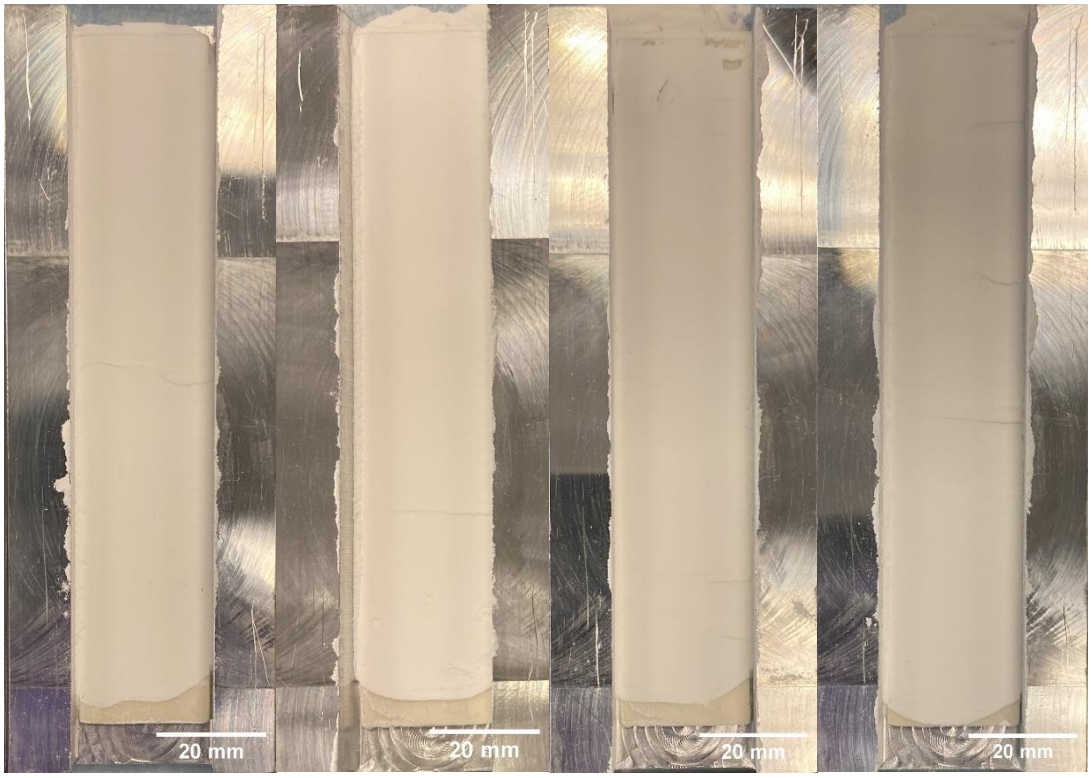

Figure 3: Plan view optical images showing surface quality of powder bed after compaction, From Left to Right: Trial 1, Trial 2, Trial 3, Trial 4

The surface quality of the powder bed was visually inspected after each compaction trial. The overall visual results for each trial are shown in Figure 3. As shown in the table, degree of compaction increased with each trial. The most common issue was a slight shifting of the powder bed during compaction, resulting in visible cracks such as the ones shown on the left in Figure 4, and in the case of trial 3, a raised section of the powder bed, shown on the right in Figure 4. It is not clear if the shifting was directly caused by the compaction and shifting of powder, or if it was due to slight rotational and side to side movements from the manual roller. Li et al. observed "surface ridges" becoming more prominent for the first approximately 10 layers for some degrees of compaction. Where waviness was seen, it then tended to stabilize after the tenth layer (Li, Pei and Ma 2021).Thus, it is also not clear if additional spreading and packing of more powder would exacerbate or reduce waviness observed in this study. However, unlike what was observed in Li et al.'s study, here the defects were not periodic. As the surface defects increased in frequency and intensity as the compaction increased, it appeared that the roller pushed the powder bed forward as it rolled. This could be due to the increased force of compaction, or due to imperfection in the roller setup. In trials 3 and 4, the force applied by the roller was limited by the force that could be applied by the operator, not by the shims. Therefore, the roller could have been able to displace laterally and longitudinally more than in trials 1 and 2. A less common, but possibly more severe issue was the sticking of small bits of compacted powder to the roller. When sticking occurred, it caused bare regions in the powder bed and altered the geometry of the roller, both of which could impact spreading of any subsequent layers. It is not clear if the behavior observed in this study would have transitioned to behavior more similar to that observed by Li et al with a further increase in the number of layers spread.

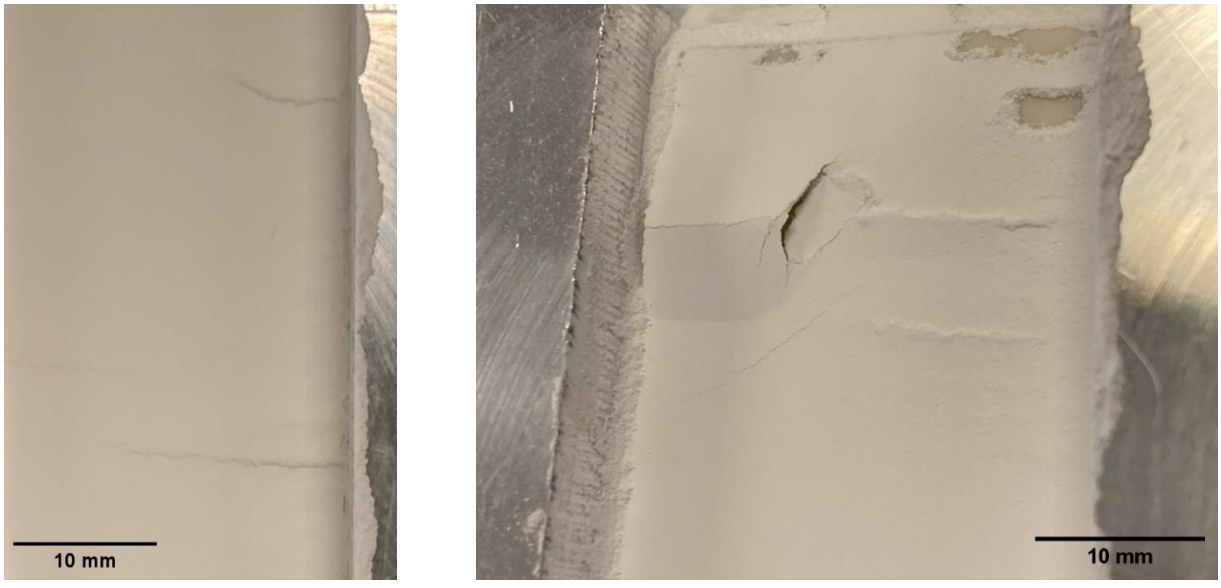

Figure 4: Visible cracks emanating from the edge of the compacted bed in Trial 4 (Left), Raised section of Trial 3 (Right). The effects of powder sticking to the roller are also apparent on the surface of the compacted powder on the right.

Figure 5 shows SEM images of the samples uniaxially pressed at 83 MPa and 41 MPa, and Figure 6 shows the SEM images of the samples pressed at 21 MPa and 10 MPa. The images

show that, while a pressure of 83 MPa is below the powder manufacturer's recommendation of a 103 MPa, this pressure and pressures as low as 21 MPa are sufficient to crush the spray-dried granules and produce a dense part after sintering. At a pressure of 10 MPa, remnant features from the original spray-dried granules are clearly visible, whereas at 21 MPa and above, the granules are fully crushed, filling in the inter-granule gaps. Figure 7 shows the SEM image of the roller-compressed granule, where the remnant features from individual granules are still visible, like the compact that was uniaxially pressed at 10 MPa. In each of these two samples, a sufficient pressure was not achieved to fully crush the spray-dried granules, causing remnants of the granules to remain visible in the final sintered part and resulting in large inter-granule pores. Inter-granule pores this large are problematic because they cannot be removed by additional sintering and they strongly affect part strength.

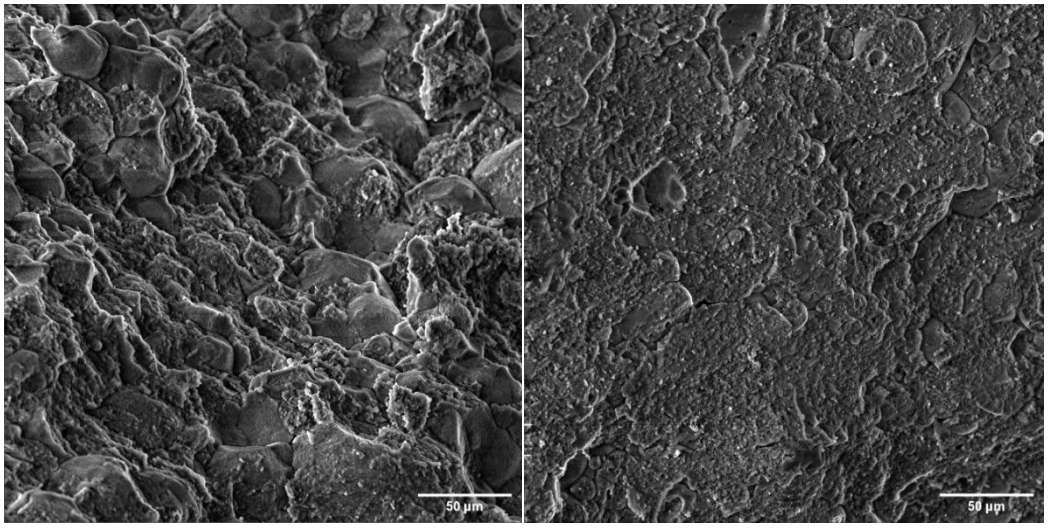

Figure 5: Images of the surfaces of parts pressed uniaxially at 83 MPa (left), 41 MPa (right)

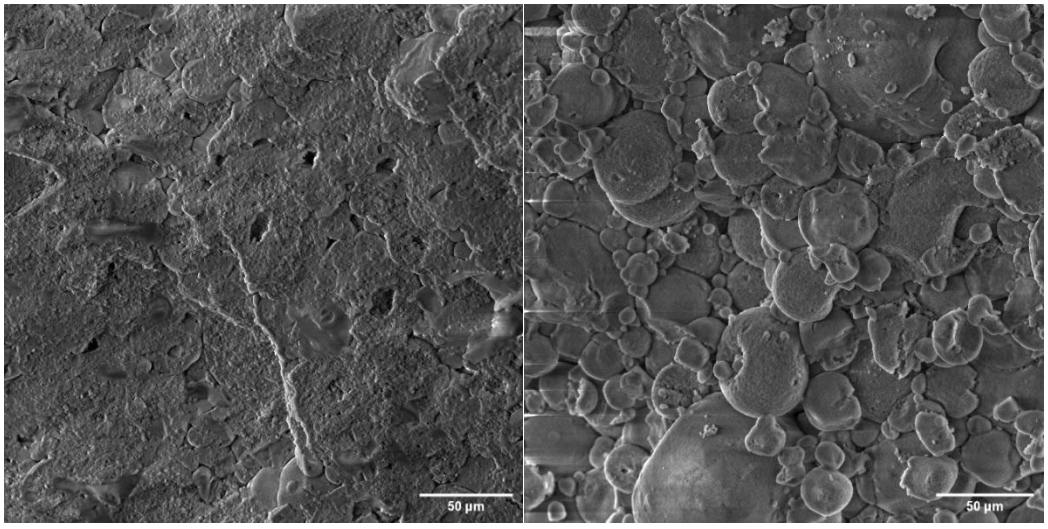

Figure 6: Images of the surfaces of parts pressed uniaxially at 21 MPa (left), 10 MPa (right)

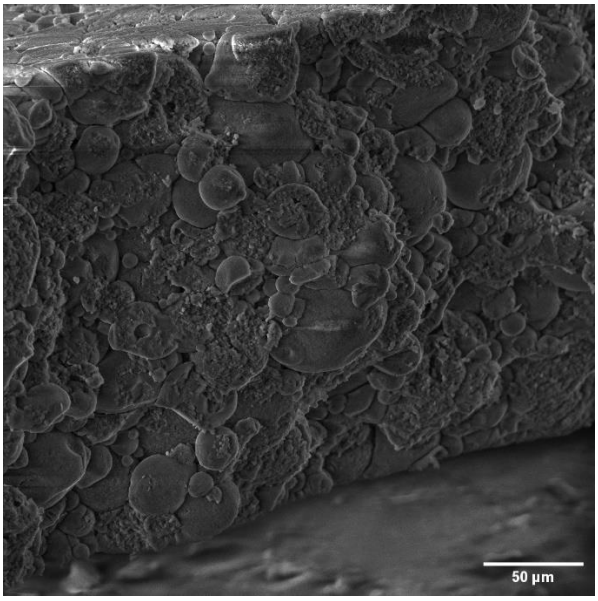

Figure 7: Surface of coupon from Trial 4 that was compressed using roller

Conclusions

In these tests, the effects of compaction via a roller on final sintered density of spray-dried alumina were studied. A manually operated roller was manufactured to control displacement of the roller and vary the degree of compaction of the powder. Coupons from compacted regions of powder bed were sintered according to supplier guidelines and compared to traditional uniaxially compacted specimens. Visual characterization via SEM suggested that the granules fully collapsed for pressures above 21 MPa. The final sintered density for all samples pressed at a pressure above 21 MPa had similar densities to the supplier-suggested pressure of 103 MPa. Roller compacted, and uniaxially pressed samples pressed at a pressure of 10 MPa that were observed in the SEM both contained remnants of the original granules, suggesting that the pressure was not high enough to fully collapse the granules.

Future work will focus on achieving higher density. This can be achieved with the current material by raising compression force. Higher compression force could be delivered with a roller design offering a mechanical advantage for compression and we are currently exploring this option. Alternatively, a higher density could also be achieved using a different material that requires less compaction force. A spray-dried powder containing a more deformable polymer binder would be beneficial, as opposed to the commercially available feedstock used in this study, which is designed for pressing at 103 MPa. Compression studies with more layers would be useful for studying surface defects in the powder bed observed here to determine if the number of defects attenuate or amplify as more layers are added.

References

Bruch, C. A. 1962. "Sintering Kinetics for the High Density Alumina Process." *American Ceramic Society Bulletin* 41 (12): 799-806. https://bulletin-archive.ceramics.org/1962-12/.

Budding, A., and T. H. J. Vaneker. 2013. "New Strategies for Powder Compaction in Powder-based Rapid Prototyping Techniques." Edited by B. Lauwers and J.P. Kruth. *Procedia CIRP* 6: 527-532. doi:10.1016/j.procir.2013.03.100.

Du, Wenchao, Xiaorui Ren, Zhijian Pei, and Chao Ma. 2020. "Ceramic Binder Jetting Additive Manufacturing: A Literature Review on Density." *Journal of Manufacturing Science and Engineering* 142 (040801): 1087-1357. doi:https://doi.org/10.1115/1.4046248.

Hagen, Deborah, Desiderio Kovar, and Joseph Beaman. 2018. "Effects of Electric Field on Selective Laser Sintering of Yttria-Stabilized Zirconia Ceramic Powder." *Solid Freeform Fabrication 2018: Proceedings of the 29th Annual International Solid Freeform Fabrication Symposium – An Additive Manufacturing Conference.* Austin, TX: University of Texas at Austin. doi:10.26153/tsw/17087.

Hagen, Deborah, Joseph Beaman, and Desiderio Kovar. 2020. "Selective laser flash sintering of 8-YSZ." *Journal of the American Ceramic Society* 103 (2): 800-808. doi:10.1111/jace.16771.

Li, Ming, Zhijian Pei, and Chao Ma. 2021. "Binder jetting additive manufacturing: observations of compaction-induced powder bed surface defects." *Manufacturing Letters* 50-53. doi:10.1016/j.mfglet.2021.04.003.

Moghdasi, Mohammadamin, Guanxiong Miao, Ming Li, Zhijian Pei, and Chao Ma. 2021. "Combining powder bed compaction and nanopowders to improve density in ceramic binder jetting additive manufacturing." *Ceramics International* 47 (24): 35378-35355. doi:https://doi.org/10.1016/j.ceramint.2021.09.077.

Sing, Swee Leong, Wai Yee Yeong, Florencia Edith Wiria, Bee Yen Tay, Ziqiang Zhao, Lin Zhao, Zhiling Tian, and Shoufeng Yang. 2017. "Direct selective laser sintering and melting of ceramics: a review." *Rapid Prototyping Journal* 23 (3): 611-623. doi:10.1108/RPJ-11-2015-0178.